Thermal and Electric Conductivities of Coulomb Crystals in Neutron Stars and White Dwarfs

D. A. Baiko and D. G. Yakovlev

Ioffe Physical Technical Institute, Russian Academy of Sciences,
Politekhnicheskaya 26, St. Petersburg, 194021 Russia

Received on May 11, 1995

Abstract

Thermal and electric conductivities are calculated for degenerate electrons scattered by phonons in a crystal made of atomic nuclei. The exact phonon spectrum and the Debye–Waller factor are taken into account. Monte Carlo calculations are performed for body-centered cubic (bcc) crystals made of C, O, Ne, Mg, Si, S, Ca, and Fe nuclei in the density range from 10^3 to 10^{11} g cm^{-3} at temperatures lower than the melting temperature but higher than the temperature at which the Umklapp processes begin to be "frozen out". A simplified method of calculation is proposed, which makes it possible to describe the results in terms of simple analytic expressions, to extend these expressions to any species of nucleus, and to consider face-centered cubic (fcc) crystals. The kinetic coefficients are shown to depend tangibly on the lattice type. The results are applicable to studies of heat transfer and evolution of the magnetic field in the cores of white dwarfs and in the crusts of neutron stars. The thermal drift of the magnetic field in the crust of a neutron star is discussed.

Published in Astronomy Letters 21 (1995) 702-709.

1 INTRODUCTION

Numerous studies have been devoted to calculations of the thermal and electric conductivities of electrons scattered by phonons in dense crystalline matter of the cores of white dwarfs and the crusts of neutron stars (see, e.g., Yakovlev and Urpin 1980; Raikh and Yakovlev 1980; Itoh *etal.*, 1984, 1993 and references therein). In particular, Raikh and Yakovlev (1982) calculated the thermal and electric conductivities by the Monte Carlo method taking into account the exact phonon spectrum in a Coulomb crystal of atomic nuclei, as well as the contribution of the Umklapp processes and the normal electron-phonon scattering processes.

Later, Itoh *etal.* (1984, 1993) performed new calculations for the same conditions taking into consideration the Debye – Waller factor. This factor describes suppression of the electron-phonon scattering for large amplitudes of ion vibrations in crystals. In their calculations, the authors used an approximate treatment of the Umklapp processes. Moreover, they fitted their results by very cumbersome formulas. In addition, all the quoted calculations were made for bcc Coulomb crystals, whereas fcc crystals may also exist in stellar matter (Section 6).

The aim of this study is to repeat the exact ("from the first- principles") Monte Carlo calculations of Raikh and Yakovlev (1982) including the Debye – Waller factor, to study the dependence of the kinetic coefficients on the lattice type, and to present the results in the form suitable for practical use. Possible applications of the results are outlined, including the thermal drift of the magnetic field in the crust of a neutron star.

2 STATEMENT OF THE PROBLEM

We will restrict ourselves to the case of sufficiently dense matter, $\rho \gtrsim AZ$ g cm^{-3} (A and Z are the mass and charge numbers of nuclei, respectively), where the electron gas is degenerate and almost ideal, while the atoms are completely ionized by electron pressure. For simplicity, we consider only one atomic species.

The state of degenerate electrons is described by the Fermi momentum $p_{\rm F} = \hbar k_{\rm F} = \hbar(3\pi^2 n_e)^{1/3}$ or by the relativistic parameter

$$x = \frac{p_{\rm F}}{m_e c} \approx 1.009 \left(\frac{\rho_6}{\mu_e}\right)^{1/3}, \tag{1}$$

where n_e is the electron number density, m_e is the electron mass, ρ_6 is the density in units of 10^6 g cm^{-3}, and μ_e is the number of baryons per electron. The electron gas is nonrelativistic ($x \ll 1$) for $\rho \ll 10^6$ g cm^{-3} and becomes ultrarelativistic ($x \gg 1$) for $\rho \gg 10^6$ g cm^{-3}.

The state of ions (nuclei) is characterized by the parameter of nonideality $\Gamma \equiv Z^2e^2/(ak_{\rm B}T)$, where $a = [3/(4\pi n_i)]^{1/3}$ is the mean separation between the nuclei, n_i is the number density of the nuclei, and $k_{\rm B}$ is the Boltzmann constant. At moderately high temperatures, the nuclei form a Coulomb crystal. A bcc crystal, which is studied in the main part of this paper (a fcc crystal is analyzed in Section 6), is the most tightly bound crystal (see, e.g., Brush *etal.* 1966). We will consider the temperature range $T_U < T < T_m$. Here, $T_U \sim T_p Z^{1/3} e^2/(\hbar v_{\rm F})$ is the temperature below which the Umklapp processes are frozen out (see below), $v_{\rm F}$ is the Fermi velocity of the electrons, and T_m and T_p are the melting and ion plasma temperatures, respectively,

$$T_m = \frac{Z^2e^2}{ak_{\rm B}\Gamma_m} \approx 1.323 \times 10^5 Z^{5/3} \left(\frac{\rho_6}{\mu_e}\right)^{1/3} \frac{172}{\Gamma_m}\ {\rm K}, \tag{2}$$

$$T_p = \frac{\hbar\omega_p}{k_{\rm B}} \approx 7.832 \times 10^6 \sqrt{\frac{Z\rho_6}{A\mu_e}}\ {\rm K}. \tag{3}$$

The crystal melts at $\Gamma = \Gamma_m \approx 172$ (Nagara *etal.* 1987). Under conditions of study, T_m is significantly lower than the electron degeneracy temperature. Strictly speaking, the melting temperature of crystals made of the lightest nuclei (H, He) decreases at high densities due to strong zero-point vibrations of the nuclei (Mochkovitch and Hansen 1979). We will not consider these nuclei. The plasma temperature T_p is determined by the ion plasma frequency $\omega_p = \sqrt{4\pi Z^2 e^2 n_i/m_i}$, where m_i is the nuclear mass. Note that the Debye temperature of the crystal is $T_{\rm D} \approx 0.45 T_p$ (Carr 1961). At $T \gtrsim T_U$, the electron-phonon scattering can be treated in the approximation of almost free electrons. If $Z \gg 1$, the main contribution to the scattering comes from the Umklapp processes. The matter is a good conductor; there are many free electrons per one ion. The latter circumstance clearly distinguishes dense stellar matter from "terrestrial" metals (see, e.g., Yakovlev and Urpin 1980). At $T \ll T_U$, the character of the electron-phonon scattering changes (Raikh and Yakovlev 1982). The Umklapp processes are frozen out: as the temperature decreases, these processes occur only in those cases where the electron momenta before and after scattering lie near intersections of the electron Fermi surface with the boundaries of the Brillouin zones (where the electron energy spectrum contains an energy gap). We do not consider temperatures $T \ll T_U$ as they are usually not important for applications.

The thermal κ and electric σ conductivities are conveniently expressed in terms of the electron effective collision frequencies ν_κ and ν_σ:

$$\kappa = \frac{\pi^2 {k_\mathrm{B}}^2 T n_e}{3 m_* \nu_\kappa} \approx 4.04 \times 10^{15} x^2 \beta T_6 \left(\frac{10^{16}\mathrm{s}^{-1}}{\nu_\kappa} \right) \frac{\mathrm{erg}}{\mathrm{cm\ s\ K}},$$
$$\sigma = \frac{e^2 n_e}{m_* \nu_\sigma} \approx 1.49 \times 10^{22} x^2 \beta \left(\frac{10^{16}\mathrm{s}^{-1}}{\nu_\sigma} \right) \frac{1}{\mathrm{s}}. \tag{4}$$

Here, $\beta = v_\mathrm{F}/c = x/\sqrt{1+x^2}$, $m_* = m_e\sqrt{1+x^2}$.

To calculate ν_κ and ν_σ, we use the well-known variational method (Ziman 1962) with the simplest trial functions that describe deviation of the electron distribution from equilibrium. For astrophysical conditions, this method was used, for example, by Flowers and Itoh (1976) and all their successors. At $T \gtrsim T_p$, this method yields an exact result, while at $T \ll T_p$, it gives an error of no more than a few percent in calculations of ν_σ and no more than a few dozen percent in calculations of ν_κ.

We describe the electron states using the scheme of extended Brillouin zones in the approximation of free electrons. In this case, the Fermi surface and the dispersion relation take the same form as those for the free electron gas. We obtain

$$\nu_{\sigma,\kappa} = \frac{e^2}{\hbar v_\mathrm{F}} \frac{k_\mathrm{B} T}{\hbar} F_{\sigma,\kappa} \approx 0.955 \times 10^{15} \frac{T_6}{\beta} F_{\sigma,\kappa} \ \ \mathrm{s}^{-1}, \tag{5}$$

where we have introduced convenient dimensionless functions

$$F_{\sigma,\kappa} = \frac{2}{t^2 S^2} \int_S \int_S \frac{\mathrm{d}S\,\mathrm{d}S'}{q^4 |\varepsilon(q)|^2} \left[1 - \frac{\beta^2 q^2}{4 k_\mathrm{F}^2} \right] \mathrm{e}^{-2W(q)}$$
$$\times\ |f(q)|^2 \sum_s [\boldsymbol{q}\boldsymbol{e}_s(\boldsymbol{k})]^2 \frac{\mathrm{e}^z}{(\mathrm{e}^z - 1)^2} g_{\sigma,\kappa}, \tag{6}$$

in which

$$t = \frac{T}{T_p} = 0.128 T_6 \left(\frac{A \mu_e}{Z \rho_6} \right)^{1/2}, \quad z \equiv z_s = \frac{\hbar \omega_s(\boldsymbol{k})}{k_\mathrm{B} T},$$
$$g_\sigma = q^2, \quad g_\kappa = q^2 - \frac{q^2 z^2}{2\pi^2} + \frac{3 {k_\mathrm{F}}^2 z^2}{\pi^2}, \tag{7}$$

Here T_6 is the temperature in units of 10^6 K, and $s = 1, 2, 3$ enumerates three branches of phonon vibrations. Integration in (6) is carried out over all possible positions of the momenta $\boldsymbol{p}$ and $\boldsymbol{p}'$ of an electron before and after scattering on the Fermi surface; $S = 4\pi {k_\mathrm{F}}^2$ is the Fermi-surface area. The quantity $\hbar\boldsymbol{q} = \boldsymbol{p} - \boldsymbol{p}'$ is the electron momentum transfer in a scattering event, and $\boldsymbol{k}$ and $\boldsymbol{e}_s(\boldsymbol{k})$ are, respectively, the wave vector and the polarization unit vector of a phonon excited or absorbed by an electron: $\pm\boldsymbol{k} = \boldsymbol{q} - \boldsymbol{K}$, where $\boldsymbol{K}$ is such a reciprocal lattice vector that $\boldsymbol{k}$ lies in the first Brillouin zone. For $\boldsymbol{k} = \boldsymbol{q}$ ($\boldsymbol{K}$=0), here occur the so-called normal scattering processes, while for $\boldsymbol{k} \neq \boldsymbol{q}$ ($\boldsymbol{K} \neq 0$), one has the Umklapp processes. The quantity $\varepsilon(q)$ in (6) is the static longitudinal dielectric function of the electron gas. It describes the screening of the Coulomb potential of nuclei by electrons. The quantity $f(q)$ is the nuclear form-factor that takes into account finite size of atomic nuclei. Finally, $W(q)$ is the Debye-Waller factor (see, e.g., Davydov (1983))

$$2W(q) = 2W(\boldsymbol{q}) = \frac{\hbar}{2m_i n_i} \sum_s \int \frac{\mathrm{d}\boldsymbol{k}}{(2\pi)^3} \frac{[\boldsymbol{q}\boldsymbol{e}_s(\boldsymbol{k})]^2}{\omega_s(\boldsymbol{k})} \mathrm{cth}\left(\frac{z_s}{2}\right), \tag{8}$$

where integration is carried out over the first Brillouin zone. Calculations show that under the conditions of interest, it is sufficient to set

$$2W(q) = \frac{1}{3}q^2 r_0^2, \quad r_0^2 = \frac{3\hbar^2}{2m_i k_\mathrm{B} T} \left\langle \frac{1}{z_s} \mathrm{cth}\left(\frac{z_s}{2}\right) \right\rangle, \tag{9}$$

where r_0^2 is the rms deviation of an ion at a crystal site. The angular brackets denote averaging over phonon frequencies and polarizations:

$$\langle f_s(\boldsymbol{k}) \rangle = \frac{1}{3V_\mathrm{B}} \sum_s \int_{V_\mathrm{B}} \mathrm{d}\boldsymbol{k}\, f_s(\boldsymbol{k}), \tag{10}$$

Here, V_B is the volume of the Brillouin zone. At $t \gg 1$, we have $\langle z^{-1}\mathrm{cth}\,(z/2)\rangle = 2u_{-2}t^2$, while at $t \ll 1$, $\langle z^{-1}\mathrm{cth}\,(z/2)\rangle = u_{-1}t$. In this case $u_n = \langle (\omega/\omega_p)^n \rangle$ are the frequency moments of the phonon spectrum.

According to (6) and (9), the Debye–Waller factor weakens the electron-phonon interaction and increases the thermal and electric conductivities. Clearly, it is important for strong ion vibrations in the lattice – near the melting point (when thermal vibrations are especially strong) and at high densities of the matter (when zero-point vibrations are strong).

3 METHOD OF CALCULATION

Thermal and electric conductivities are calculated by 4D integration in (6) over all orientations of the electron momenta $\boldsymbol{p}$ and $\boldsymbol{p}'$ on the Fermi surface. The Monte Carlo method has been used for numerical integration.

Initially we have calculated the phonon spectrum for a bcc Coulomb crystal immersed in a uniform compensating electron-charge background. The frequencies $\omega_s(\boldsymbol{k})$ and polarization unit vectors $\boldsymbol{e}_s(\boldsymbol{k})$ of phonons of three modes ($s = 1, 2, 3$) are determined from the system of equations composed of the elements of the dynamic matrix (Kohen and Keffer 1955; Carr 1962). Extensive tables of the dynamic matrix elements have been calculated for values of $\boldsymbol{k}$ in different points of a primitive cell of the first Brillouin zone. To determine the phonon parameters for an arbitrary wave vector $\boldsymbol{k}$, we have interpolated the tabulated data and then solved the system of equations. Near the center of the Brillouin zone, for $k \ll q_D$ (where $q_D = (6\pi^2 n_i)^{1/3}$ is the radius of the sphere with a volume equal to that of the Brillouin zone), we have used the well-known asymptotic expressions (Kohen and Keffer 1955) for the dynamic matrix elements. In the approximation of a uniform electron background, for $k \ll q_D$, two phonon modes ($s = 1$ and 2) prove to be acoustic ($\omega_s \sim \omega_p k/q_D$), while the third ($s = 3$) is optical ($\omega_s \approx \omega_p$). Response of the electron background is important only for the frequency of the third mode for $k \ll q_D$. Under the action of the response, the optical mode transforms into an acoustic one (Pollock and Hansen 1973). To allow for this effect, the frequency $\omega_3(\boldsymbol{k})$ obtained for the uniform electron background has been multiplied by $k/\sqrt{k^2 + k_{\rm TF}{}^2}$, where

$$k_{\rm TF} = k_{\rm F}\sqrt{\frac{4e^2}{\pi\hbar v_{\rm F}}} \tag{11}$$

is the inverse radius of electron screening of a charge in plasma.

In our calculations, we have used the static longitudinal dielectric function $\varepsilon](q)$ of a degenerate relativistic electron gas obtained by Jancovici (1962). The simplest (see, e.g., Itoh *etal.* 1993) form-factor has been chosen,

$$f(q) = \frac{3}{(qr_c)^3}\left[\sin(qr_c) - qr_c\cos(qr_c)\right], \tag{12}$$

corresponding to the uniform charge distribution in the proton core (of radius r_c) of an atomic nucleus. In the density range of interest (see below), the radii of nuclei do not change under the ambient pressure, and we can use the standard formula $r_c = 1.15 \times 10^{-13} A^{1/3}$ cm.

Initially we have calculated the Debye – Waller factor (9) for the bcc lattice. The results closely match those of Itoh @et al.@ (1984, 1993). However, we have obtained a simpler fitting equation:

$$2W(q) = \frac{q^2\hbar}{m_i\omega_p}\left(1.3995\exp(-2.7256t) + t\,\frac{4.9801 + 13.00\times 61.099t^2}{1 + 61.099t^2}\right). \tag{13}$$

This expression gives an error less than 1% for any q. We have calculated the integrals (6) for eight elements: ^{12}C, ^{16}O, ^{20}Ne, ^{24}Mg, ^{28}Si, ^{32}S, ^{40}Ca and ^{56}Fe. Unlike Itoh *etal.* (1984, 1993), we have not considered H and ^{4}He. For hydrogen, the Umklapp processes are not allowed at all, and the kinetic coefficients require a separate treatment. The helium melting temperature (Mochkovitch and Hansen 1979) is likely to be lower than the temperature T_U at which the Umklapp processes are frozen out, which is beyond the scope of our study (Section 2). We have calculated F_κ and F_σF@k for the electron relativistic parameters x = 0.1, 0.3, 1, 3, 10, and 30 and for the dimensionless temperatures t = 0.02, 0.04, 0.08, 0.2, 0.4, 0.8, 2, 4, 8, and 20. The selected values of x correspond to the density range from approximately 2×10^3 g cm$^-$3. Unlike Itoh *etal.* (1984, 1993), we have not considered lower densities ρ, since the approximation of complete ionization does not hold at these ρ (see, e.g., Yakovlev and Urpin 1980). For carbon, we have excluded the value x = 30, because at such a high density carbon is instantaneously burned in pycnonuclear reactions (Yakovlev 1994). For all elements, we have also excluded those t at which $T > 2T_m$ (see (2)). Calculations of F_κ and F_σ for each element at fixed x and t have required up to 500 000 configurations in "Monte Carlo chains" (choices of orientations of the momenta $\boldsymbol{p}$ and $\boldsymbol{p}'$ on the Fermi surface) to achieve an acceptable accuracy of 5 - 10In all the cases of interest, an inclusion of the nuclear form-factor (allowance for the non-point distribution of the nuclear charge) has virtually no effect on the final result. The finite sizes of nuclei become important only at $\rho \gtrsim 10^{12}$ g cm$^-$3.

4 NUMERICAL RESULTS AND THEIR ANALYTIC ANALYSIS

For practical applications, it is useful to fit the functions F_σ and F_κ by simple analytic expressions similar to those proposed by Yakovlev and Urpin (1980) and Raikh and Yakovlev (1982). Under the conditions of interest, the main contribution to the electron scattering comes from the Umklapp processes. The Fermi surface is crossed by many boundaries of the Brillouin zones, and we may set in (6)

$$\sum_s [\boldsymbol{q}\boldsymbol{e}_s(\boldsymbol{k})]^2 \frac{z^n \mathrm{e}^z}{(\mathrm{e}^z - 1)^2} \approx q^2 t^2 \pi^n G_n(t), \tag{14}$$

$$G_n(t) = \frac{1}{\pi^n t^2} \left\langle \frac{z^n \mathrm{e}^z}{(\mathrm{e}^z - 1)^2} \right\rangle, \tag{15}$$

where $n = 0$ or 2, and the angular brackets imply averaging (10).

The functions $G_n(t)$ were calculated by Yakovlev and Urpin (1980), who also proposed simple fit formulas:

$$\begin{aligned} G_0(t) &= \frac{u_{-2} t}{\sqrt{t^2 + a_0}}, \\ G_2(t) &= \frac{t}{\pi^2 (t^2 + a_2)^{3/2}}. \end{aligned} \tag{16}$$

The coefficients in (16) are chosen in such a way to reproduce the asymptotic expressions for $t \ll 1$ and $t \gg 1$; equations (16) describe $G_n(t)$ with an error less than 10frequency moments of the phonon spectrum (Section 2). For a bcc lattice, we have $u_{-2}^{(bcc)} = 13.00$ (see, e.g., Mochkovitch and Hansen 1979), $a_0^{(bcc)} = 0.0174$ and $a_2^{(bcc)} = 0.0118$.

Using the approximation (14), from (6) we obtain

$$\begin{aligned} F_\sigma &= \frac{G_0(t)}{k_F^2} \int_{q_{min}}^{2k_\mathrm{F}} q\, \mathrm{d}q\, \frac{|f(q)|^2}{|\varepsilon(q)|^2} \left(1 - \frac{\beta^2 q^2}{4k_F^2}\right) \mathrm{e}^{-2W}, \\ F_\kappa &= F_\sigma + \frac{G_2(t)}{k_F^2} \int_{q_{min}}^{2k_\mathrm{F}} q\, \mathrm{d}q\, \frac{|f(q)|^2}{|\varepsilon(q)|^2} \left(1 - \frac{\beta^2 q^2}{4k_F^2}\right) \left(\frac{3k_F^2}{q^2} - \frac{1}{2}\right) \mathrm{e}^{-2W}. \end{aligned} \tag{17}$$

Following Yakovlev and Urpin (1980), we have taken into account that the simplified expression (14) is valid only for the Umklapp processes. Therefore, the region of integration over the electron momentum transfer q in a scattering event is limited by a minimum momentum q_{min}. We set $q_{min} = q_\mathrm{D} = (6\pi^2 n_i)^{1/3}$, where q_D is the radius of a sphere with the volume V_B. For $q \lesssim q_\mathrm{D}$, the normal scattering processes dominate.

1D integrals (17) are readily calculated numerically. However, they can also be approximately expressed in an analytic form. Indeed, finite sizes of nuclei are unimportant, under the conditions of interest (Section 3), and we may take $f(q) = 1$. The dielectric function $\varepsilon(q)$ of an electron gas differs slightly from unity for $q \gtrsim k_\mathrm{TF}$ (11). Only for $q \ll k_\mathrm{TF}$ does the quantity $|\varepsilon(q)|^2$ sharply increase: the electron screening becomes important, giving rise to an effective cutoff of the integrals for low $q \lesssim k_\mathrm{TF}$. Simple estimates show that $k_\mathrm{TF} \ll q_\mathrm{D}$ in all the cases of study except for those of the lowest density ($\rho \sim 10^3$ g cm^{-3}). At $\rho \lesssim ZA$ g cm^{-3}, the electron screening would become extremely important, but our approach becomes invalid. In particular, the condition of complete ionization is violated (Section 2). In calculating the integrals (17) approximately, the electron screening may be taken into account by shifting the lower integration limit q_{min}. We set $q_{min}^2 \sim q_\mathrm{D}^2 + {k_\mathrm{TF}}^2$ and $\varepsilon = 1$ for $q > q_{min}$. The integrals can then be taken:

$$F_\sigma = G_0(t)[2R_0(s_\sigma) - \beta^2 R_1(s_\sigma)], \tag{18}$$

$$\begin{aligned} F_\kappa &= G_0(t)[2R_0(s_\kappa) - \beta^2 R_1(s_\kappa)] \\ &+ \frac{1}{2} G_2(t)[\beta^2 R_1(s_\kappa) - 3\beta^2 R_0(s_\kappa) - 2R_0(s_\kappa) + 3R_2(s_{1\kappa})]. \end{aligned} \tag{19}$$

Here, we have introduced the functions

$$\begin{aligned} R_0(s) &= \frac{1}{\alpha}(\mathrm{e}^{-\alpha s} - \mathrm{e}^{-\alpha}), \\ R_1(s) &= \frac{2}{\alpha^2}[\mathrm{e}^{-\alpha s}(1+\alpha s) - \mathrm{e}^{-\alpha}(1+\alpha)], \\ R_2(s) &= \mathrm{E}(\alpha s) - E(\alpha), \end{aligned} \tag{20}$$

in which $\mathrm{E}(x)$ is the integral exponent, $\alpha = 4r_0^2 k_\mathrm{F}{}^2/3$ is defined by r_0 in the Debye–Waller factor(9) , and $s = q_{min}^2/(2k_\mathrm{F})^2$. It is convenient to take somewhat different lower limits q_{min} in the functions F_κ and F_σ (see below). In our case, $q_{min} \ll k_\mathrm{F}$ and $s \ll 1$. Note that $\mathrm{E}(q)$ can be calculated conveniently using the simple fit formula

$$\begin{aligned} \mathrm{E}(q) &= \int_q^\infty \frac{\mathrm{d}y}{y}\,\mathrm{e}^{-y} \\ &\approx \exp\left(-\frac{q^4}{q^3+0.1397}\right)\left[\ln\left(1+\frac{1}{q}\right) - \frac{0.5772}{1+2.2757q^2}\right]. \end{aligned} \tag{21}$$

With a mean error of about 1%, the Debye–Waller parameter α can be fitted by

$$\alpha = \alpha_0\left(\frac{1}{2}u_{-1}\mathrm{e}^{-9.100t} + tu_{-2}\right), \quad \alpha_0 = \frac{4m_e^2c^2}{k_\mathrm{B}T_p m_i}x^2 \approx 1.683\sqrt{\frac{x}{AZ}}, \tag{22}$$

where u_{-1} is another frequency moment of the phonon spectrum. For a bcc lattice, $u_{-1}^{(bcc)} = 2.800$ (Mochkovitch and Hansen 1979).

If $\alpha \ll 1$, the Debye–Waller factor is unimportant. Since $s \ll 1$, in this case we obtain

$$R_0(s) \approx R_1(s) \approx 1, \quad R_2 \approx \ln\left(\frac{1}{s}\right). \tag{23}$$

These formulas correspond to the approximation used by Yakovlev and Urpin (1980), as well as by Raikh and Yakovlev (1982). The inclusion of the Debye–Waller factor weakens the electron scattering, and the functions R_0, R_1 and R_2 become smaller than (23). The functions (20) completely determine the dependence of electric and thermal conductivities on the Debye–Waller factor.

Let us compare the approximate analytic expressions (18) – (22) for F_σ and F_κ with the results of our numerical calculations (Section 3). The values of F_σ appear to be fitted by equation (18) with an error not larger than the error of the computations if we set in the functions $R_0(s_\sigma)$ and $R_1(s_\sigma)$

$$s_\sigma = s_\mathrm{D} + s_\mathrm{TF}, \tag{24}$$

$$
\begin{aligned}
s_{\rm D} &= \frac{q_{\rm D}^2}{4k_{\rm F}^2} = \left(\frac{1}{4Z}\right)^{2/3}, &(25)\\
s_{\rm TF} &= \frac{k_{\rm TF}^2}{4k_{\rm F}^2} = \frac{1}{137\pi\beta}. &(26)
\end{aligned}
$$

If one uses the same parameter @s for thermal conductivity

$$
s_\kappa = s_{1\kappa} = s_\sigma = s_{\rm D} + s_{\rm TF}, \tag{27}
$$

formulas (19) – (22) fit the calculated values of F_κ with a mean error of 10% for all eight chemical elements and all x and t. The approximation (27) is least accurate for light elements, primarily for carbon (for it, the mean error is about 15%, and the maximum error of ≈30% is obtained at $x = 10$ and $t = 0.2$). The accuracy of the F_κ fit can be improved, on average, by a factor of about 1.5, if we take

$$
\begin{aligned}
s_\kappa &= s_{\rm D}\zeta + s_{\rm TF}\xi,\\
s_{1\kappa} &= s_{\rm D}\zeta_1 + s_{\rm TF}\xi_1,\\
\zeta &= 0.101 + 0.0305Z, \;\; \xi = 3.84 + \frac{834}{Z^3},\\
\zeta_1 &= \frac{2.66}{Z^{0.122}} - 1, \;\; \xi_1 = 1.456 - \frac{257.4}{Z^2} + \frac{4874}{Z^4}. &(28)
\end{aligned}
$$

For applications, we recommend to use (24) and (27) because their accuracy is quite acceptable. It is clear from the derivation of equations (24) and (27) that they can also be applied to other chemical elements. Equations (28) are more accurate, but they hold only for $6 \le Z \le 26$.

The functions F_σ and F_κ were previously calculated with allowance for the Debye–Waller factor by Itoh *etal.* (1984, 1993). These authors started from approximate equations (17), whereas we have performed our numerical calculations using the general but much more complicated equations (6). Our calculations confirm the validity of simplified equations (17). Hence, our numerical results agree, within the calculational errors, with those of Itoh *etal.* (1984, 1993). We have thus proved the validity of the approximate calculations of electric and thermal conductivities based on equations (14) and (17). Furthermore, we have carried out an analytic analysis of equations (17). This has enabled us to obtain the simple fit equations (18) – (27) valid to all chemical elements considered. As follows from their derivation, these equations are also valid for other elements (see above). Itoh *etal.* (1984, 1993) also fitted their results by analytic expressions, but their expressions are very cumbersome. They include 56 adjustable parameters for each element and do not allow one to extend the results directly to other elements.

The quantities F_σ and F_κ, calculated with and without allowance for the Debye–Waller factor, are shown in Figs. 1 and 2. Including the Debye–Waller factor increases the electric and thermal conductivities of matter. The effect is especially pronounced in the cases where the amplitude of ion vibrations in a lattice cite is large, that is, near the melting point (where thermal vibrations are strong) and at high densities (where zero vibrations are important; Fig. 2). At $T \sim T_m$ the Debye–Waller factor increases the kinetic coefficients by a factor of $2-4$.

At $t \gtrsim 1$, the electron-phonon scattering becomes quasi-elastic (the energy transfer in a scattering event is much smaller than kBT). Using (17), (20) and (22), one can easily show that in this case a single effective collision frequency can be introduced for both electric and thermal conductivities:

$$\begin{aligned} \nu_0 &= \nu_\sigma = \nu_\kappa = \frac{e^2}{\hbar v_\mathrm{F}} \frac{k_\mathrm{B} T}{\hbar} F_0, \\ F_0 &= F_\sigma = F_\kappa = \frac{2u_{-2}}{\alpha^2} \left[\alpha \left(1 - \mathrm{e}^{-\alpha}\right) - \beta^2 \left(1 - (1+\alpha)\,\mathrm{e}^{-\alpha}\right) \right]. \end{aligned} \tag{29}$$

We have taken into account that $s\alpha \ll 1$ in virtually all the cases studied. Equation (29) is a generalization of the similar expression obtained by Yakovlev and Urpin (1980) without allowance for the Debye–Waller factor.

For $t \gg 1$ and $\alpha \gg 1$, equations (22) and (29) yield the simple expression

$$\nu_0 = \frac{2m_* e^4 Z}{3\pi\hbar^3}. \tag{30}$$

In this limiting case, the collision frequency of electrons is temperature independent and close to a similar frequency (see, e.g., Yakovlev and Urpin 1980) in the Coulomb liquid ($T > T_m$). Formally, the collision frequency (30) would be equal to the frequency in the liquid if the Coulomb logarithm were equal to $\Lambda = 0.5$.

5 THERMAL DRIFT OF THE MAGNETIC FIELD

The effective collision frequency (29) defines, in particular, the thermal drift of the magnetic field $\boldsymbol{B}$ in the neutron star crust (Urpin and Yakovlev 1980). Recall that the thermal drift is caused by the heat flux emerging from the stellar interior. For simplicity, we consider a weakly magnetized degenerate electron gas in which $\omega_B \tau_0 \ll 1$. Here, $\omega_B = eB/(m_* c)$ is the gyrofrequency of electrons with energies equal to the Fermi energy, and $\tau_0 = 1/\nu_0$ is the effective relaxation time. Under these conditions, the heat flux is almost unaffected by the magnetic field, and the thermal drift is determined by the Hall component of the specific thermal electromotive force. The thermal drift velocity u is parallel to the heat flux Q and for $t \gtrsim 1$ is equal to

$$u = \frac{2\eta Q}{n_e p_{\rm F} v_{\rm F}} \approx 72\eta \frac{\sqrt{1+x^2}}{x^5} \left(\frac{T_e}{10^6\ {\rm K}}\right)^4 \ \frac{\rm m}{\rm yr}, \tag{31}$$

$$\eta = \frac{1}{2}\,\frac{\partial \ln(\tau_0(\varepsilon)\varepsilon^{-1})}{\partial \ln p}. \tag{32}$$

Here, we set $Q = \sigma T_e^4$, where T_e is the effective temperature of the stellar surface. The numerical coefficient $\eta \sim 1$ is determined by the logarithmic derivative with respect to the electron momentum. Once the derivative in (32) is taken, $p = p_{\rm F}$ should be set. Basically, η can have different signs, depending on the mechanism of electron scattering. In the Coulomb liquid ($T > T_m$), according to Urpin and Yakovlev (1980), $\eta > 0$, and the thermal drift is directed outward. In crystalline matter, from (32) at $t > 1$ we obtain

$$\eta = \frac{1}{2} - \beta^2 + \frac{3\alpha r_1 - 2\alpha\beta^2 r_2 + 3(\beta^2 - \beta^4) r_0}{6r_0 - 3\beta^2 r_1}, \tag{33}$$

$$r_0 = \frac{1}{\alpha}\left(1 - {\rm e}^{-\alpha}\right), \quad r_1 = \frac{2}{\alpha^2}\left[1 - (1+\alpha){\rm e}^{-\alpha}\right],$$

$$r_2 = \frac{3}{\alpha^3}\left[2 - (2 + 2\alpha + \alpha^2){\rm e}^{-\alpha}\right], \tag{34}$$

Plots of η against density in the neutron star envelope with the temperature $T = 8\times 10^7$ K are shown in Fig. 3. This temperature corresponds to $T_e \sim 10^6$ K. The coefficient η calculated for the crystal without allowance for the Debye–Waller factor is indicated by long dashes. It can be obtained from (33) and (34) in the limit $\alpha \to 0$: $\eta = (2 - 3\beta^2)/(4 - 2\beta^2)$ (Urpin and Yakovlev 1980). In this approximation, η is positive in a low-density electron gas (for $v_{\rm F}^2/c^2 < 2/3$) but becomes negative at higher densities. However, Fig. 3 shows that at $T \sim T_m$ with allowance for the Debye–Waller factor, η remains positive and close to a similar coefficient in the liquid phase. With increasing density and at a fixed temperature, t and η decrease. Formally, at a sufficiently high density, equation (33) gives negative η, but this occurs only at $t \lesssim 1$, when the formula becomes invalid. In the validity range of (33) and for typical values of the parameters, η remains positive, and the thermal drift is directed outward. The calculation of η at $t < 1$ is very complicated and it is beyond the scope of this study.

6 FACE-CENTERED COULOMB CRYSTALS

The preceding astrophysical calculations of electric and thermal conductivities have been all performed for body-centered Coulomb crystals that are most tightly bound. In addition to bcc crystals, fcc and simple cubic Coulomb crystals can in principle exist. The binding energy of an ion in a Coulomb crystal of any type is $U = -\zeta Z^2 e^2/a$ (Brush *etal.* 1966), where a is the ion sphere radius (Section 2), and the coefficients ζ are equal ζ_{bcc}= 0.895929, ζ_{fcc}=0.895874 and ζ_{sc}=0.880059. The binding energies for bcc and fcc crystals are very close to each other. The difference in the ion energies (in units of thermal energy) is $(U_{bcc} - U_{fcc})/(k_{\rm B}T) \approx -0.000055\Gamma$, where Γ is the nonideality parameter (Section 2). Near the melting point, $T \approx T_m$, we have $\Gamma \approx 172$ and $(U_{bcc} - U_{fcc})/(k_{\rm B}T) \approx -0.01$. Consequently, in addition to bcc crystals, fcc crystals can be be formed in many cases.

In Section 4, we have justified the validity of a simplified calculation of thermal and electric conductivities based on equations (14) and (17). Let us apply this approach to fcc crystals. Using (15) and (17), we can calculate the functions F_σ and F_κ. In this case, the type of lattice affects the functions $G_0(t)$ and $G_2(t)$, as well as the Debye–Waller parameter α. Using the results of Kohen and Keffer (1955), we have created a computer code for calculating the phonon spectrum. The spectrum resembles the phonon spectrum of a bcc crystal. In particular, there are two acoustic and one optical modes near the center of the Brillouin zone, but the frequencies of acoustic phonons are somewhat lower. As a result, the frequency moments $u_{-1}^{(fcc)} = 4.03$ and $u_{-2}^{(fcc)} = 28.8$ are larger than those for a bcc crystal. We have also calculated some other frequency moments: $u_1^{(fcc)}$=0.462, $u_4^{(fcc)}$=0.267. The integration over the Brillouin zone in the expressions for $G_0(t)$, $G_2(t)$ and α has been carried out by the simplified method proposed by Mochkovitch and Hansen (1979). The results can be fitted by the same equations (16) and (22) as for the bcc lattice but with other values of constants: $a_0^{(fcc)}$=0.00505, $a_2^{(fcc)}$=0.00461. The fit accuracy turns out to be of the same order of magnitude. All equations (18) - (28) for F_κ and F_σ remain valid.

The plots of F_κ and F_σ versus t for the bcc and fcc lattices made of iron nuclei are given in Fig. 4. The curves are similar but the peaks at $t \sim 1$ are much more pronounced for the fcc lattice, which is a result of a softer spectrum of acoustic phonons. At higher t, the curves approach each other since they are described by the common asymptote (30).

A simple cubic lattice is appreciably more weakly bound than a bcc or fcc lattice. In addition, the phonon frequencies in some crystallographic directions of a simple cubic lattice turn out to be complex, i.e., such a lattice is unstable. This is a common and well-known (Born 1940) property of cubic lattices composed of particles interacting through central forces.

7 CONCLUSION

We have calculated the electric and thermal conductivities of degenerate relativistic electrons scattered by phonons in Coulomb bcc and fcc crystals made of atomic nuclei taking into account the Debye – Waller factor. The results of these calculations are valid at densities 10^3 g cm^{-3} $\lesssim \rho \lesssim 10^{11}$ g cm^{-3}. For bcc crystals, the calculations are performed by the Monte Carlo method using the exact formulas. Our results confirm the validity of the approximate approach used by Itoh *etal.* (1984, 1993). An analytic analysis of the results has enabled us to describe them by the simple fit expressions (17) – (28) and extend the calculations to the fcc lattice. It is shown that thermal and electric conductivities are sensitive to the lattice type.

One might expect our results to be also applicable at sufficiently low densities, 1 g cm^{-3} $\lesssim \rho \lesssim 10^3$ g cm^{-3}, where the pressure ionization of atoms is incomplete. In this density range, the charge number Z of nuclei should be replaced in all the above expressions with an effective charge number $Z_{eff} \leq Z$ determined by electron screening of the nuclear charge. However, no reliable calculations of Z_{eff} have been made as yet.

Our results are valid for degenerate cores of white dwarfs and to outer degenerate envelopes of neutron stars. First of all, these results can be useful in studying the thermal evolution of these objects (cooling, nuclear burning of accreted matter) and the evolution of their magnetic field (ohmic dissipation, generation under thermomagnetic effects). In particular, we have shown in Section 5 that an inclusion of the Debye–Waller factor strongly affects the thermal drift of the magnetic field in the crust of a neutron star.

The results can easily be generalized to higher densities, 10^{11} g cm^{-3} $\lesssim \rho \lesssim 10^{14}$ g cm^{-3}. To do this, the functions F_σ and F_κ should be calculated with allowance for finite sizes of atomic nuclei for realistic models of superdense matter of subnuclear density. We plan to consider this in a separate work.

ACKNOWLEDGMENTS

We wish to thank M.E. Raikh and V.A. Urpin for helpful discussions. This study was supported in part by the Russian Basic Research Foundation (Project Code 93-02-2916), ESO (Grant A-01- 068), and ISF (grant R6-A000). One of the authors (D.A. Baiko) is also grateful to the mayor of St. Petersburg (Grant 661 for support of the youth's scientific work in the High Education System) and to ISF (students' grant 555s).

REFERENCES

Born, M., Proc. Cambr. Phil. Soc., 1940, vol. 36, p. 160.

Brush, S.G., Sahlin, H.L., and Teller, E., J. Chem. Phys., vol. 45, p. 2102.

Carr, W.J., Phys. Rev., 1962, vol. 122, p. 1437.

Cohen, M.N. and Keffer, K., Phys. Rev., 1955, vol. 99, p. 1128.

Davydov, A.S., *Fizika Tverdogo Tela* (Solid State Physics), Moscow: Nauka, 1983.

Itoh, N., Kohyama, Y., Matsumoto, N., and Seki, M., Astrophys. J., 1984, vol. 285, p. 758; erratum 404, 418.

Flowers, E. and Itoh, N., Astrophys. J., 1976, vol. 206, p. 218.

Jankovici, B., Nuovo Cimento, 1962, vol. 25, p. 428.

Mochkovitch, R. and Hansen, J.-P., Phys. Lett., vol. A73, p. 35, 1979.

Nagara, H., Nagata, Y., Nakamura, T., Phys. Rev., 1987, vol. A36, p. 1859.

Pollock, E.L. and Hansen, J.-P., Phys. Rev., 1973, vol. 8A, p. 3110.

Raikh, M.E. and Yakovlev, D.G., Astrophys. Space Sci., 1982, vol. 87, p. 193.

Urpin, V.A. and Yakovlev, D.G., Sov. Astron., 1980, vol. 24, p. 425.

Yakovlev, D. G., Acta Phys. Polonica, 1994, vol. B25, p. 401.

Yakovlev, D.G. and Urpin, V.A., Sov. Astron., 1980, vol. 24, p. 303.

Ziman, J.M., Electrons and Phonons, Oxford: Clarendon, 1960.

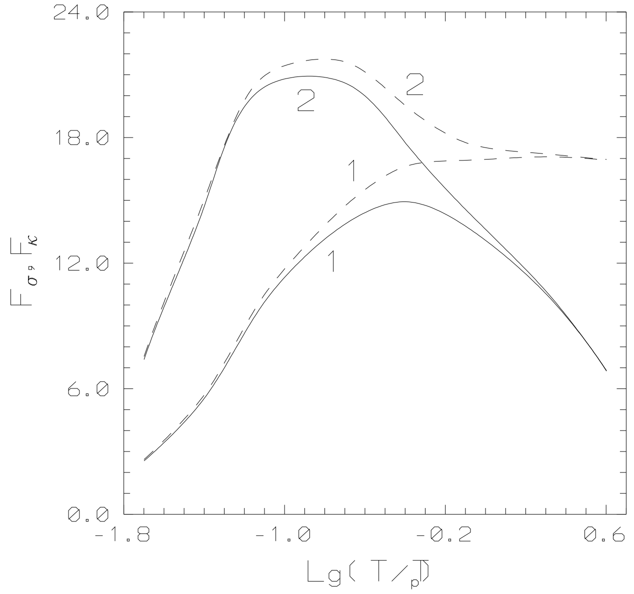

Figure 1: F_σ (curves 1) and F_κ (curves 2) versus $t = T/T_p$ for a crystal composed of ^{56}Fe at the density $\rho = 2.1 \times 10^6$ g cm^{-3} ($x = 1$) with (solid lines) and without (dashed lines) allowance for the Debye–Waller factor.

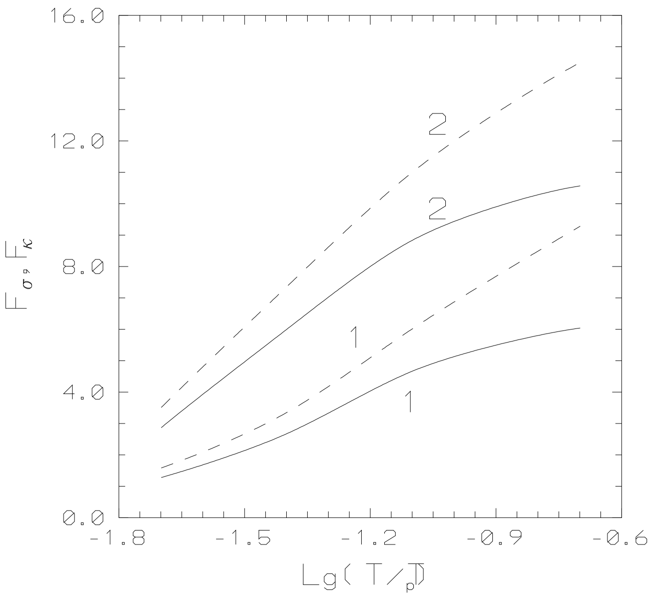

Figure 2: Same as in Fig. 1 but for ^{12}C nuclei at $\rho = 5.26 \times 10^7$ g cm^{-3} ($x = 3$).

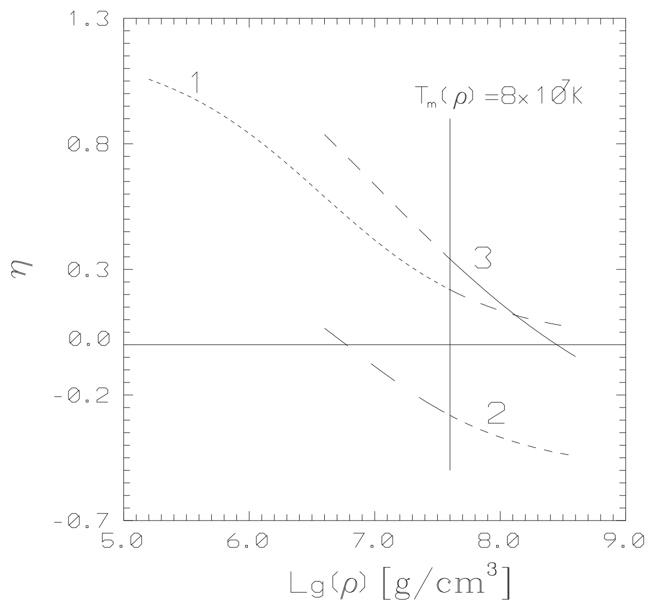

Figure 3: The coefficient η that determines the thermal drift velocity of the magnetic field (see (31)) as a function of density at $T = 8 \times 10^7$ K for matter composed of ^{56}Fe nuclei. Curve 1 corresponds to the Coulomb liquid (Urpin and Yakovlev 1980), curve 2 to a crystal without allowance for the Debye–Waller factor, and curve 3 to a crystal with allowance for this factor. The vertical line shows the density above which solidification occurs.

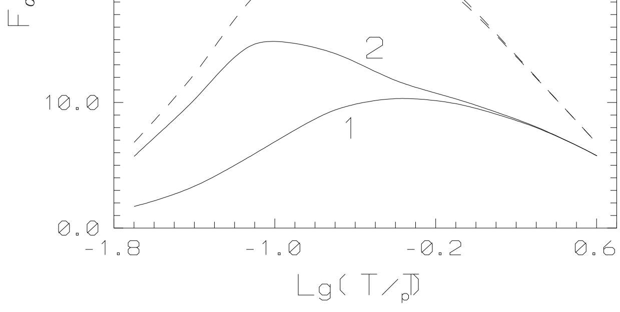

Figure 4: Same as in Fig. 1, for bcc (solid lines) and fcc (dashed lines) crystals with allowance for the Debye–Waller factor.